Published in final edited form as:
J Phys Chem C Nanomater Interfaces. 2007 May 3; 111(17): 6398–6404. doi:10.1021/jp0675429.

Amelogenin Promotes the Formation of Elongated Apatite Microstructures in a Controlled Crystallization System

Lijun Wang[†], **Xiangying Guan**[†], **Chang Du**[‡], **Janet Moradian-Oldak**[‡], and **George H. Nancollas**[*,†]

[†]Department of Chemistry, University at Buffalo, The State University of New York, Amherst, New York 14260

[‡]Center for Craniofacial Molecular Biology, School of Dentistry, University of Southern California, Los Angeles, California 90033

Abstract

The organic matrix in forming enamel consists largely of the amelogenin protein self-assembled into nanospheres that play a pivotal role in controlling the oriented and elongated growth of highly ordered apatitic crystals during enamel biomineralization. However, the mechanisms of amelogenin-mediated mineralization have not yet been fully elucidated. Here we report that amelogenin dramatically accelerates the nucleation kinetics by decreasing the induction time in a dose-dependent manner in a controlled constant composition (CC) in vitro crystallization system. Remarkably, at very low protein concentrations, elongated microstructures which are similar in appearance to apatitic crystals in enamel were formed at relatively low supersaturations, through interfacial structural match/synergy between structured amelogenin assemblies and apatite nanocrystallites. This heterogeneous crystallization study provides experimental evidence to support the concept that templating by amelogenin very early in the crystallization process facilitates the formation of developing enamel crystals.

Introduction

Biomineralized materials are highly organized from the molecular to the nano- and macroscales, often in a hierarchical manner, with intricate nanoarchitectures that ultimately make up a myriad of different functional hard tissues.[1,2] In biomineralization, a significant aspect of biological control over mineral formation is through protein/inorganic recognition and interaction,[3] such as in the biosynthesis of dental structures.[4] The studies on proteins extracted from biomineralized tissues that can control the nucleation, orientation, polymorphism, and morphology of the mineral phase have prompted a number of biomimetic studies in the presence of natural proteins and synthetic organic molecules.[5-7]

In vitro biomimetic studies on the formation of apatite crystals, including octacalcium phosphate (OCP),8 hydroxyapatite (HAP),9 and fluoroapatite (FAP)10 in the presence of amelogenin have attempted to unveil the mechanism of enamel formation through the analysis of amelogenin-mineral interaction. Supramolecular assembly of amelogenin protein into nanospheres has been recognized as a key factor in controlling the oriented and elongated growth of enamel apatite crystals in matrix-mediated mineralization.11-14 It has also been suggested that cooperative assembly and interactions between forming crystals and assembling

[*]Corresponding author. Tel: +1-716-645-6800 ext. 2210. Fax: +1-716-645-6947. E-mail: ghn@buffalo.edu.

proteins is pivotal to biomineralization processes.15,16 Here, we used a precisely controlled CC crystallization method sensitive to ion concentration changes at the nanomolar level in order to study amelogenin activity at relatively low concentrations, in controlling apatite nucleation and crystal growth. This provides reliable rates of crystal growth and induction times of nucleation,[17] enabling studies of apatite crystallization in the presence of low concentrations of amelogenin. We found that amelogenin protein can nucleate and direct the formation of elongated ribbon-like microstructures which are similar in appearance to apatitic crystals in enamel, via interfacial match/synergy between structured amelogenin assemblies and apatite nanocrystallites in the octacalcium phosphate (OCP) supersaturated solution system.

Experimental Section

Amelogenin Protein Purification and Characterization

The recombinant expression plasmid (pETp172) was kindly provided by Dr. James P. Simmer at the University of Michigan.[18] Recombinant porcine amelogenin rP172 was expressed in *Escherichia coli* strain BL21-codon plus (DE3-RP, Strategene), purified by ammonium sulfate precipitation, and reverse-phase high performance liquid chromatography (HPLC, C4-214TP510 column, Vydac, Hesperia, CA). Protein purity was assessed by SDS-PAGE and analytical reverse-phase HPLC (C4-214TP54 column) and determined to be more than 98%. The protein has 172 amino acids and is an analogue to the full-length porcine P173 lacking the N-terminal methionine and a phosphate group on Ser16.[19]

Constant Composition of OCP Nucleation/Crystal Growth

OCP nucleation experiments were made in double-walled Pyrex glass vessels maintained at 37.0 ± 0.05 °C. The relative supersaturation, σ, is defined as eq 1:

$$\sigma = S - 1 = \left(\frac{\mathrm{IAP}}{K_{\mathrm{sp}}}\right)^{1/v} - 1 \tag{1}$$

in which v (=16) is the number of ions in a formula unit of the OCP growing phase, S is the supersaturation ratio, and IAP and K_{sp} are the ionic activity and solubility products, respectively. The solubility product of the OCP used in these calculations was taken as 2.51×10^{-99} $\mathrm{mol}^{16}\ \mathrm{l}^{-16}$.[20] The relative degrees of supersaturation and ionic activities were calculated from the experimental total concentrations using the speciation programs described previously based on expressions for ion-pair and complex formation constants, mass balance, and electroneutrality.[21] Supersaturated reaction solutions ([$CaCl_2$] = 2.5 mmol l^{-1}, [KH_2PO_4] = 1.88 mmol l^{-1}, and [NaCl] = 0.139 mol l^{-1} for σ_{OCP} = 1.45; and [$CaCl_2$]=3.62 mmol l^{-1}, [KH_2PO_4]=2.72 mmol l^{-1}, and [NaCl]=0.135 mol l^{-1} for σ_{OCP} = 2.32) were prepared by the slow mixing of calcium chloride (0.02 mol l^{-1}) and potassium dihydrogen phosphate (0.02 mol l^{-1}) with the ionic strength maintained at 0.15 mol l^{-1} by the addition of sodium chloride solution. Lyophilized amelogenin proteins were dissolved in 0.5 or 1 mL triple-distilled water (pH 5.5 and room temperature) and stirred by 15 min ultrasonication, and then added to reaction solutions. The pH (6.800) was adjusted immediately following the addition of amelogenin ([protein] = 0.5-5.0 μg mL^{-1}) to the required value by the very slow addition of a 0.06 mol l^{-1} potassium hydroxide solution to avoid local concentration effects and unwanted spontaneous precipitation. A pH electrode (Orion 91-01) coupled with a single-junction Ag/AgCl reference electrode (Orion 90-01) along with a pH meter (Orion 720A) was used to monitor changes in hydrogen ion activities. Nitrogen gas, presaturated with water vapor, was bubbled continuously through the reaction solutions during pH adjustment and crystallization experiments.

The initial consumption of crystal lattice ions, accompanying nucleation, was detected by a change in the hydrogen ion activity sensed by a glass electrode. The lowering of the pH was used to trigger the simultaneous addition of two titrant solutions from stepper-motor-driven burets that served to maintain constant the pH, the concentrations of calcium and phosphate, and the ionic strength of the reaction solutions. The concentrations of the titrant solutions were calculated using mass balance and electroneutrality expressions. Titrant I consisted of calcium chloride and sodium chloride at concentrations given by eq 2 and 3, respectively:

$$T_{\mathrm{Cacl}_2}=2W_{\mathrm{Cacl2}}+4C_{\mathrm{eff}} \tag{2}$$

$$T_{\mathrm{Nacl}}=2W_{\mathrm{Nacl}}-8C_{\mathrm{eff}} \tag{3}$$

Titrant II contained potassium dihydrogen phosphate and potassium hydroxide with concentrations given by eq 4 and 5, respectively.

$$T_{\mathrm{KH2PO4}}=2W_{\mathrm{KH2PO4}}-3C_{\mathrm{eff}} \tag{4}$$

$$T_{\mathrm{KOH}}=2W_{\mathrm{KOH}}-5C_{\mathrm{eff}} \tag{5}$$

In eqs 2-5, T and W are the titrant and metastable supersaturated reaction solution concentrations, respectively, and C_{eff} is the effective concentration of added titrants with respect to OCP, or the moles of OCP formed per liter of mixed titrants. A suitable C_{eff} was chosen to provide convenient titrant volumes; the value of C_{eff} for this study was usually 0.25 mmol l^{-1}.

During the experiments, the constancy of concentrations was verified by analysis of filtered aliquots (0.22 μm Millipore filters) for calcium by atomic absorption spectrometry (Perkin-Elmer Atomic Absorption Spectrometer 3100) and for phosphate spectrophotometrically as the vanadomolybdate complex (Hewlett-Packard, 8452A, Diode Array Spectrophotometer). In all cases, the concentrations remained constant throughout the precipitation reactions to within ±1.5%.

Mineral Characterization

Crystallites for SEM investigation (Hitachi S-4000 FESEM) were separated from the solution by filtration at the end of the experiments and dried at room temperature. SEM images were collected using a primary beam voltage at 20 keV. Experiments were made at least three times. TEM images and electron diffraction patterns were done using the JEOL TEM 2010 (working voltage, 200 keV).

Dynamic Light Scattering (DLS) Analysis

The particle size distribution of rP172 in calcium or phosphate-containing solutions was analyzed by DynaPro99E MS/X-TC dynamic light scattering instrument equipped with a solid-state laser operating at 655 nm and a temperature controlled MicroSampler at 37 °C as previously described.[18] The autocorrelation function of the signal from the scattered intensity was measured by a multichannel digital correlator. The normalized intensity correlation function was analyzed by a regularization method to give the information on the distribution of the exponential decay function with decay rate Γ. The translational diffusion coefficient can

be determined through $\Gamma = Dq^2$ where q is the scattering vector. The hydrodynamic radius R_H is calculated from D via the Stokes-Einstein equation, $R_H = kT/(6\pi\eta D)$, where k is the Boltzmann constant and η the solvent viscosity at temperature T.[22] The data collection was continued for 60 runs with the acquisition time of 10 s. The validity of the data was determined by the parameters including amplitude, baseline limit and the sum of squares error, as well as the autocorrelation curves. Typically, more than 40 valid data can be obtained from 60 runs. The detected hydrodynamic radii from the individual runs were grouped into 13 categories: <10, 10-20, 20-30, 30-40..., 90-100, 100-200, 200-300, and >300 nm. The occurrence rates of different categories were used to represent the particle size distribution in this heterogeneous system.

Results and Discussion

The Effect of Amelogenin on Nucleation Kinetics of Calcium Phosphate

It is widely accepted that the physiologically most important calcium phosphate phase in mature tooth enamel crystals is carbonate-containing fluoridated hydroxyapatite [$Ca_{10}(PO_4)_6(OH)_2$, HAP].[23] OCP [$Ca_8H_2(PO_4)_6{\cdot}5H_2O$] is a metastable phase of HAP, and whether enamel apatite is formed by direct crystallization from supersaturated solution or through one or multiple intermediate phase(s) such as amorphous, brushite or OCP remains unsettled.[24] Therefore, we chose one of possible phases, OCP, for nucleation and crystal growth experiments at a relatively low supersaturation (σ_{OCP}=1.45). CC experimental conditions included pH (6.800), ionic strength (0.15 mol l^{-1}) and reaction temperature (37 °C) close to physiological conditions. The reaction solution was stable for more than 12 h in the absence of amelogenin, following which OCP crystals precipitated in the reaction cell. The CC nucleation results in the present study show that amelogenin dramatically accelerates the nucleation by decreasing the induction time in a dose-dependent manner (Figure 1). The induction time for pure supersaturated solution was 748 ± 25 (n = 4) minutes. The presence of a 0.5, 1.25 or 5.0 μg mL^{-1} concentration of amelogenin decreased the induction times to 678 ± 22 (n = 3), 523 ± 20 (n = 3) and 407 ± 17 (n = 3) minutes, respectively.

The reproducibility of the measured induction periods depends both upon their magnitude and the thermodynamic driving force. In the induction region, the solution concentrations and pH were unchanged and the volume, dV, of added titrant remained essentially zero, confirming the absence of mineral nucleation or growth. Once nucleation took place, the reduction in solutionpH with time due to deprotonation of $H_2PO_4^-$ and HPO_4^{2-} ions associated with the formation of mineral precipitates was monitored. Corresponding pH profiles (Figure 1) with and without protein additive showed a characteristic nucleation reaction process. No kinetic inhibition was observed in the presence of amelogenin; instead, the pH curves indicated a marked decrease in the time required for OCP crystallization.

In most cases, biomineralization is associated with the formation of a new phase via nucleation followed by growth.[25] As the first step of biomineralization, nucleation therefore plays an important role in building a complex structure. In the process of nucleation, increase in the size of an embryo must overcome a free energy nucleation barrier, ΔG_{homo}, for a given $\Delta\mu$ ($\Delta\mu$, chemical potential difference between the actual state and the equilibrium state) before it can reach a critical radius, r_c, and become a stable growing crystal. In the case of homogeneous nucleation, the effect of the substrate is negligible, so the barrier for a spherical nucleus is given by[26-28]

$$\Delta G_{homo} = \frac{16\pi\gamma_{cf}{}^3\Omega^2}{3\Delta\mu^2} \quad (6)$$

and the critical size of the nuclei is

$$r_c=\frac{2\gamma_{cf}}{\Delta\mu} \tag{7}$$

$$\Delta\mu=kT\ln(1+\sigma) \tag{8}$$

where γ_{cf} is the interfacial free energy between the mineral nucleus (c) and the fluid (f), Ω is the volume per growth unit, k is the Boltzmann constant, T is the absolute temperature andσ is the relative supersaturation of solution.

In the presence of organic substrates, the nucleation barrier is reduced to

$$\Delta G^*=\Delta G_{homo} f(m)\,(0\le f\le 1) \tag{9}$$

where $f(m)$ is the interfacial correlation factor describing the lowering of the nucleation barrier due to the presence of the substrate. The factor $f(m)$ varies from 0 to 1, depending on the correlation and structural match between the nucleating phase and the substrate.[29] When the interaction between the nucleating phase and the substrate is optimal, $f(m) \to 0$. Conversely, if the interfacial correlation is very poor, $f(m) \to 1$, and the substrate exerts almost no influence on the nucleation barrier. Taking into account the effect of the substrate on both the nucleation barrier and the transport process, the nucleation rate is given by[30]

$$J=(R^s)^2N^0 f''(m)\,[f(m)]^{0.5}B\quad \exp\left[-\frac{\Delta G_{homo}}{kT}f(m)\right] \tag{10}$$

where R^s and N^0 are the radius of curvature and the density of the substrates, respectively, B is the kinetic constant.

The technical difficulties involved in directly evaluating crystal nucleation have led to other approaches to initial crystallization events, one of the most common ways to characterize the kinetics of nucleation is to measure the induction period (t_s) prior to nucleation at different supersaturations. This approach allows investigation of the modulation of the initial events in calcium phosphate crystallization by additives. By definition,[30] the nucleation rate J can be expressed as eq 11:

$$J=1/(tsV) \tag{11}$$

where V is the volume of the system. Combining eq 10 and 11 yields eq 12:

$$\ln\quad t_s=\frac{\kappa f(m)}{[\ln(1+\sigma)]^2}-\ln\left\{V(R^s)^2N^0 f''(m)\,[f(m)]^{1/2}B\right\} \tag{12}$$

where $\kappa[=(16\pi\gamma_{cf}{}^3\Omega^2/3(kT)^3)]$, remains constant under a given set of conditions. In the amelogenin/OCP nucleation system, since amelogenin serves as “seeds” or organic substrates for OCP nucleation, the change of the amelogenin concentration is equivalent to the change of

N^0 in eqs 10 and 12, and this will lead to significantly shorter induction times (Figure 1) with a consequent promotion of nucleation. Moreover, at low supersaturations, the nucleation barrier is very high (see eq 6 and 8) and the rate will be substantially raised if the barrier is lowered. Therefore, heterogeneous nucleation, accompanied by a small $f(m)$ (eq 9) with strong interactions and a very good structural match between protein substrate and crystal, will be kinetically favored.[28] An increase of supersaturation will drive the substrates/minerals from an interfacial structural matching state (a lower $f(m)$) to a state of greater mismatch (higher $f(m)$). This phenomenon is referred to as supersaturation-driven interfacial structural mismatch.[31] Therefore, we chose a relatively low supersaturation in our nucleation system in order to acquire a slow and well controlled mineralization by magnifying the amelogenin additive/template effect on the nucleation at relatively low protein concentrations. The nucleation kinetics results support the template effect of amelogenin (Figure 1).

Formation of Elongated Microstructures via Co-assembly of Amelogenin and Apatite Nanocrystallite

Prior to the appearance of an observable amount of the new phase, the pH remained constant. However, after the initial induction periods, the pH decreased and apatite-like aggregates were formed from the solutions both in the absence and presence of amelogenin at the same supersaturation (σ_{OCP}=1.45) (Figure 2). SEM and EDS (energy dispersion spectrum) investigations of samples collected following the induction periods indicated that plate-like OCP crystallites formed in the absence of amelogenin were aggregated in a random manner (Figure 2a). EDS revealed a Ca/P ratio of 1.33 ± 0.05 (n = 5, number of crystals), consistent with the OCP chemical stoichiometry of the supersaturated solution (inset in Figure 2a). However, in the presence of amelogenin at 5.0 μg mL^{-1}, the calcium phosphate crystallites showed a remarkable change of microstructure. Ordered ribbon-like crystals with a higher aspect ratio, ~60 μm in length, 10 ± 3 μm (n = 7) in width and 100-200 μnm in thickness, were formed (Figure 2b). Interestingly, EDS of the microribbon crystals showed a Ca/P ratio of 1.66 ± 0.08 (n = 5, number of the ribbon-like crystals), suggesting HAP (inset in Figure 2b) rather than OCP.

Consistent with the SEM observations, transmission electron microscopic (TEM) examination revealed that the ribbons were stable and their shape was retained on the copper grid after they were air-dried (Figure 3a). HRTEM images showed that the less mineralized areas (in the red rectangle marked in Figure 3a) of the ribbons consisted of ~3-4 nm nanocrystallites indicated by dotted circles in Figure 3b, and the selected-area electron diffraction (SAED) pattern confirmed the presence of diffraction arcs corresponding to the (002), (310), (311) and (004) planes of HAP (inset in Figure 3b). In addition, in the more mineralized areas (a white rectangle marked in Figure 3a) of the ribbons, the primary nanoparticles were not randomly oriented, but were ordered into aggregated (larger) clusters with parallel crystallographic axes (Figure 3c and inset in Figure 3c). The measured lattice spacing ~0.346 nm corresponds to the (002) HAP lattice plane (Figure 3c), indicating preferential alignment of the HAP crystals with their c axes along the long axis of the ribbons shown by the arrow in Figure 3c. This suggests that amelogenin controlled the interfacial structural match between apatite nanocrystallites and amelogenin protein substrates during the slow nucleation process.

When the nucleation barrier was overcome, the second, crystal growth, stage of the phase transition began. Figure 4a shows a typical CC crystal growth curve after the long induction time. The lowering of the pH triggered the simultaneous addition of two titrant solutions to maintain constant the pH, the concentrations of calcium and phosphate, and the ionic strength of the reaction solutions. A more rapid titrant addition reflected the exponential growth of crystals on the nuclei formed in the heterogeneous nucleation stage (Figure 4a). SEM shows that apatite crystals were grown thickly in the presence of 5.0 μg mL^{-1} amelogenin, but retained

the ribbon-like morphology (Figure 4b). EDS spectra of the mineral crystals revealed a Ca/P ratio of 1.68 ± 0.07 (n = 5, number of the ribbon-like crystals), consistent with HAP (inset in Figure 4b).

In accordance with the theoretical prediction, at a high supersaturation (σ_{OCP} = 2.32), the induction times for supersaturated solutions in the absence and presence of 5.0 μg mL^{-1} amelogenin, 90 ± 15 (n = 3) and 79 ± 10 (n = 3) minutes, respectively, show no significant change; less ordered structures were formed when compared to those formed at σ_{OCP} =1.45 (Figure 2b, 3a and 4b). Notably, the structures are more ordered in the presence of amelogenin (Figure 5b) when compared to the control (in the absence of 5.0 μg mL^{-1} amelogenin) (Figure 5a). The similar induction times for the less ordered structures formed at higher supersaturation can be explained by supersaturation-driven interfacial structural mismatch.[28,31] With increase of supersaturation, the interfacial correlation factor $f(m)$ will increase abruptly at certain supersaturations, corresponding to a transition from an ordered structure to a less ordered and structurally mismatched mineral/organic substrate interface,[28] amelogenin exerts only a weak influence on the nucleation barrier. This observation may constitute direct evidence that at higher supersaturations, some nuclei without the interactions with amelogenin may form too rapidly to be organized. This evidence highlights the importance of amelogenin/inorganic nanocrystallite interactions. The crystallites obtained at a relatively low supersaturation show a very good structural match/synergy. Mineralization therefore leads to an ordered structure.

Amelogenin molecules can spontaneously form nanosphere structures under a wide variety of conditions.[32] Monomers and discrete oligomers such as dimers, trimers, and hexamers were detected in the diluted protein solutions at 20 °C.[11] Figure 6 showed that under our experimental conditions used for OCP crystallization (pH 6.800, 37 °C, and I = 0.15 mol l^{-1}) amelogenin, at very low concentration (5.0 μg mL^{-1}), form oligomers and small nanospheres with R_H of 3.3 to 9.2 nm, and then larger assemblies with 60-90 nm. Oligomerization of amelogenin molecules occurs mainly by means of hydrophobic interaction, which is further enhanced at 37 °C.11›32 Moreover, as previously suggested[11] the amelogenin molecule can fold into a unique globular form that preserves a bipolar nature derived from its primary structure. The hydrophilic C-terminal (-Thr-Lys-Arg-Glu-Glu-Val-Asp) “tail” is exposed on the surface of the molecule as well as on the surface of the small oligomers creating structured domains with which apatite nanoocrystallines can preferentially interact. Moradian-Oldak et al. have shown that stable clusters of apatite crystals were formed via molecular self-association of the full-length amelogenin molecules (40 μg mL^{-1}), that effectively adhered to the growing crystals through the hydrophilic c-terminal segment.[33] Beniash et al. have shown that HAP crystallites can organize with their c-axes into parallel arrays, in the presence of 1 mg mL^{-1} full-length amelogenin, while the protein without the hydrophilic c-terminal did not have any effect on crystal organization.[34] These results have implied that the C-terminal domain is essential for the alignment of the crystals into parallel arrays.[34]

A recent solid-state nuclear magnetic resonance study confirmed a direct amelogenin-apatite interaction through the hydrophilic C terminus and orienting the charged COOH-terminal region of the amelogenin protein on the HAP surface, optimized to exert control on developing enamel crystals.[35] Therefore, under our experimental conditions the presence of structured amelogenin assemblies with their negatively charged surfaces will facilitate apatite nucleation by selectively binding with Ca^{2+} or calcium phosphate clusters and hence by producing, locally, a high degree of supersaturation.[36] The nature and strength of the interaction of amelogenin with apatite crystals or calcium ions has important implications not only in controlling crystal nucleation, but also in regulating the orientation and the size of the growing crystals (with large length-to-width and small width-to-thickness ratios).[37] In the case where amelogenin micro-ribbons were used as templates for crystallization, amelogenin could initially stabilize the nuclei and apatite crystallite growth along the c-axis and directly control the manner in which

the nanospheres assemble into arrays of nanochain structures.[11] Linear arrays of spherical substructures have been also detected in the enamel extracellular matrix in vivo.[38-40] Fusion of enamel crystallites in the early stages of mineral formation has been proposed to explain the unusual long crystals formed in mature enamel.[41]

Our proposed hypothetical model for the formation of mesoscale organized mineralized structures in vitro involves a step-by-step mechanism of ordered co-assembly of amelogenin oligomers (small nanospheres) and apatite nanocrystallites. It is schematically presented in Figure 7. In the absence of amelogenin, the primary apatite nanocrystallites or critical nuclei can grow by uncontrollable ion attachment and aggregation to form random aggregates (Figure 7a). However the formation of organized microstructures involves more complicated mesoscale transformations (mesocrystal formations).[42] In this process, nanocrystallites are also formed, but they can bind with the hydrophilic "tails" of amelogenin nanospheres to form organic-inorganic hybrid building blocks which then co-assemble and aggregate in a controlled manner at relatively low supersaturations to form highly organized HAP ribbon-like crystallites (Figure 7b).

Banfield et al. suggested an aggregation-based crystal growth mechanism in biomineralization products of iron-oxidizing bacteria, in which adjacent 2-3 nm particles aggregate and rotate so their structures adopt parallel orientations in three dimensions.[43] Based on the aggregation-based growth mechanism, most of the ~3-4 nm diameter particles formed in solution and either attached to surrounding negatively charged amelogenin or flocculated to form colloidal aggregates. In our in vitro experimental model, in addition to lowering the nucleation barrier, amelogenin oligomers will reduce random Brownian motion-driven particle collisions. Jiggling of nano-particles by Brownian motion may also allow adjacent particles to rotate to find the low-energy configuration represented by a coherent particle-particle interface.[43] Zhu et al. demonstrated, by molecular dynamics simulation, the rotation of particles within aggregates to achieve parallel orientations and it may also be driven by short-range interactions between adjacent surfaces.[44]

Crystal growth by the aggregation-based mechanism has important implications for subsequent materials reactivity.[43] Phase stability can be particle size-dependent, so crystal growth can promote phase transformation.[45,46] Phase transformation is also induced if initial precipitates are metastable. Schwertmann et al. showed that recrystallization and transformation were enhanced by particle aggregation.[47] The transformation of OCP to HAP may be initiated by raising the pH from 6.5 to >7.4. Recent $^{31}P\{^{1}H\}$ NMR data suggest that water molecules enter the hydration layers of OCP crystals by the hydrolysis reaction $HPO_4^{2-} + OH^- = PO_4^{3-} + H_2O$, which accounts for the deprotonation of the HPO_4^{2-} ions during the transformation.[48] However, in our CC system, the pH remained unchanged before and after the nucleation stage and the detailed mechanism of OCP to HAP transformation remains unknown.

Conclusions

We have shown that amelogenin dramatically accelerates the nucleation of apatite by decreasing the induction time in a dose-dependent manner, suggesting that in the presence of amelogenin as substrate, the charged COOH-terminal region may be important in the specific apatite/protein binding. This binding will lower the nucleation energy barrier for a given $\Delta\mu$. Remarkably, at very low protein concentrations (0.5-5.0 μg mL^{-1}), amelogenin oligomers are able to direct the alignment of apatite crystals along the *c*-axis to form the ribbon-like crystals which are similar in appearance to apatitic crystals in enamel. This heterogeneous nucleation which corresponds to a structural match between mineral and organic substrate will promote an ordered and complex mineralized structure, providing experimental evidence that substrate templating is important and strongly support the view that amelogenin controls the formation

of developing enamel crystals at the early stages. Understanding the protein-mediated mineralization and in vitro assembly at the bio-inorganic interface will be a useful guide for biomimetic structures constructed by co/self-assembly of tailor-made peptide sequences.

Acknowledgments

We thank Liping Guo for assistance in obtaining transmission electron microscopy data and their analysis and Christopher Abbott for protein purification. This work was supported by NIH Grants DE03223 to GHN and DE13414 to JMO.

References and Notes

(1). Lowenstam, HA.; Weiner, S. On Biomineralization. Oxford University Press; Oxford: 1989.

(2). Mann, S. Biomimetic Materials Chemistry. VCH; New York: 1996.

(3). Seeman NC, Belcher AM. Proc. Natl. Acad. Sci. U.S.A 2002;99:6452.

(4). Paine ML, Snead ML. J. Bone Miner. Res 1996;12:221. [PubMed: 9041053]

(5). Walsh D, Hopwood JD, Mann S. Science 1994;264:1576. [PubMed: 17769602]

(6). Hartgerink JD, Beniash E, Stupp SI. Science 2001;294:1684. [PubMed: 11721046]

(7). Füredi-Milhofer H, Moradian-Oldak J, Weiner S, Veis A, Mintz KP, Addadi L. Connect. Tissue Res 1994;30:251. [PubMed: 7956204]

(8). Iijima M, Moradian-Oldak J. Calcif. Tissue Int 2004;74:522. [PubMed: 15354860]

(9). Hunter GK, Curtis HA, Grynpas MD, Simmer JP, Fincham AG. Calcif. Tissue Int 1999;65:226. [PubMed: 10441656]

(10). Habelitz S, Kullar A, Marshall SJ, Denuesten PK, Balooch M, Marshall GW, Li W. J. Dent. Res 2004;83:698. [PubMed: 15329375]

(11). Moradian-Oldak J, Du C, Falini G. Eur. J. Oral Sci 2006;114(Suppl 1):289. [PubMed: 16674701]

(12). Veis, A. Biomineralization, ReViews in Mineralogy and Geochemistry. Dove, PM.; De Yoreo, JJ.; Weiner, S., editors. Vol. 54. The Mineralogical Society of America; Washington, DC: 2003. p. 249

(13). Fincham AG, Moradian-Oldak J, Simmer JP. J. Struct. Biol 1999;126:270. [PubMed: 10441532]

(14). Aichmayer B, Margolis HC, Rigel R, Yamakoshi Y, Simmer JP, Fratzl P. J. Struct. Biol 2005;151:239. [PubMed: 16125972]

(15). Colfen H, Mann S. Angew. Chem., Int. Ed 2003;42:2350.

(16). Margolis HC, Beniash E, Fowler CE. J. Dent. Res 2006;85:775. [PubMed: 16931858]

(17). Tomson MB, Nancollas GH. Science 1978;200:1059. [PubMed: 17740700]

(18). Ryu OH, Fincham AG, Hu CC, Zhang C, Qian Q, Bartlett JD, Simmer JP. J. Dent. Res 1999;78:743. [PubMed: 10096449]

(19). Fincham AG, Moradian-Oldak J. Biochem. Biophys. Res. Comm 1993;197:248. [PubMed: 8250931]

(20). Shyu LJ, Perez L, Zawacki S, Heughebaert JC, Nancollas GH. J. Dent. Res 1983;62:398.

(21). Koutsoukos P, Amjad Z, Tomson MB, Nancollas GH. J. Am. Chem. Soc 1980;102:1553.

(22). Harding SE. Methods Mol. Biol 1994;22:97. [PubMed: 8312999]

(23). Brown, WE. Tooth Enamel II. Stack, MV.; Fearnhead, RW., editors. John Wright Ltd.; Bristol, U.K.: 1965. p. 11

(24). Miake Y, Shimoda S, Fukae M, Aoba T. Calcif. Tissue Int 1993;53:249. [PubMed: 8275353]

(25). Mutaftschiev, B. Handbook of Crystal Growth. North-Holland; Amsterdam: 1993. p. 187-248.

(26). Chernov, AA. Modern Crystallography III: Crystal Growth. Springer-Verlag; Berlin: 1984.

(27). Söhnel O, Mullin JW. J. Cryst. Growth 1978;44:377.

(28). Liu XY, Lim SW. J. Am. Chem. Soc 2003;125:888. [PubMed: 12537485]

(29). Liu XY. Langmuir 2000;16:7337.

(30). Liu, XY. AdVances in Crystal Growth Research. Sato, K.; Nakajima, K.; Furukawa, Y., editors. Elsevier; Amsterdam: 2001. p. 42

(31). Jiang H, Liu XY, Zhang G, Li Y. J. Biol. Chem 2005;280:42061. [PubMed: 16251185]

(32). Moradian-Oldak J, Leung W, Fincham AG. J. Struct. Biol 1998;122:320. [PubMed: 9774536]
(33). Moradian-Oldak J, Tan J, Fincham AG. Biopolymers 1998;46:225. [PubMed: 9715666]
(34). Beniash E, Simmer JP, Margolis HC. J. Struct. Biol 2005;149:182. [PubMed: 15681234]
(35). Shaw WJ, Campbell AA, Paine ML, Snead ML. J. Biol. Chem 2004;279:40263. [PubMed: 15299015]
(36). Hunter GK, Bader SM. J. Theor. Biol 1989;138:195. [PubMed: 2558258]
(37). Iijima M, Moriwaki Y, Wen HB, Fincham AG, Moradian-Oldak J. J. Dent. Res 2002;81:69. [PubMed: 11820371]
(38). Robinson C, Fuchs P, Weatherell JA. J. Cryst. Growth 1981;53:160.
(39). Robinson C, Shore RC, Wood SR, Brooks SJ, Smith DAM, Wright JT, Connell S, Kirkham J. Connect. Tissue Res 2003;44(Suppl 1):65. [PubMed: 12952176]
(40). Robinson C, Connell S, Kirkham J, Shore R, Smith A. J. Mater. Chem 2004;14:2242.
(41). Travis DF, Glimcher MJ. J. Cell Biol 1964;23:447. [PubMed: 14245432]
(42). Cölfen H, Antonietti M. Angew. Chem., Int. Ed 2005;44:5576.
(43). Banfield JF, Welch SA, Zhang HT, Ebert T, Penn RL. Science 2000;289:751. [PubMed: 10926531]
(44). Zhu HL, Averback RS. Philos. Mag. Lett 1996;73:27.
(45). McHale JM, Auroux A, Perrotta AJ, Navrotsky A. Science 1997;277:788.
(46). Zhang H, Banfield JF. J. Mater. Chem 1998;8:2073.
(47). Schwertmann U, Friedl J, Stanjek HJ. J. Colloid Interface Sci 1999;209:215. [PubMed: 9878155]
(48). Tseng Y, Mou C, Chan JCC. J. Am. Chem. Soc 2006;128:6909. [PubMed: 16719471]

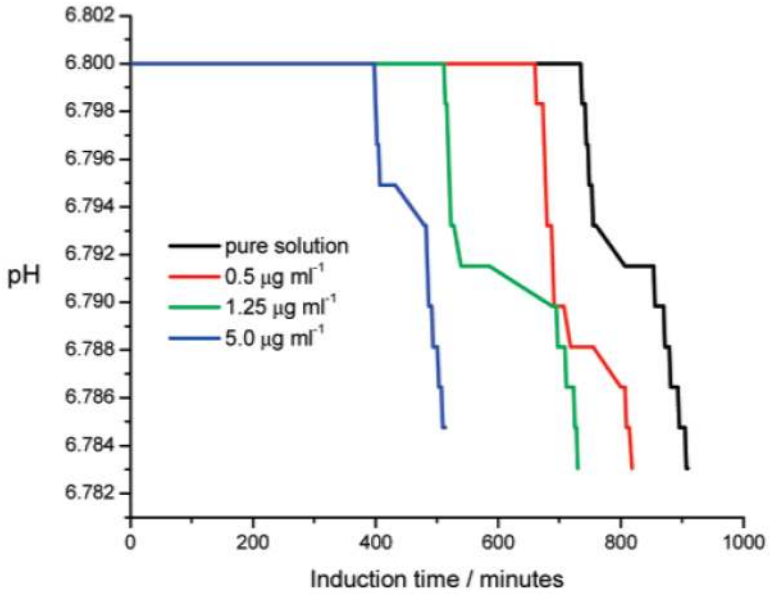

Figure 1.

pH curves for apatite nucleation in the absence and the presence of amelogenin. Amelogenin dramatically accelerates the nucleation by decreasing the induction time in a dose-dependent manner (σ_{OCP} = 1.45, pH 6.800, and 37 °C).

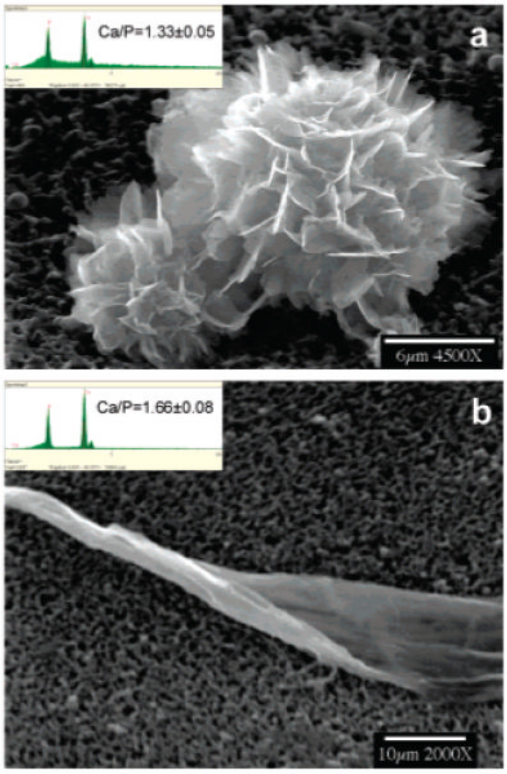

Figure 2.
Crystal morphological characterization. (a) SEM image of OCP crystals nucleated in the absence of amelogenin and collected from the bulk solution by filtration following the induction period. EDS of apatite crystals showing a Ca/P ratio of 1.33 ± 0.05 (n = 5, number of crystals), as expected for OCP (inset). (b) SEM image of organized ribbon-like crystals nucleated in the presence of 5.0 μgmL^{-1} amelogenin collected from the bulk solution by filtration after the induction period. EDS of microribbon crystals showing a HAP Ca/P ratio of 1.66 ± 0.08 (n = 5, number of crystals) rather than OCP (inset) (σ_{OCP} = 1.45, pH 6.800, and 37 °C).

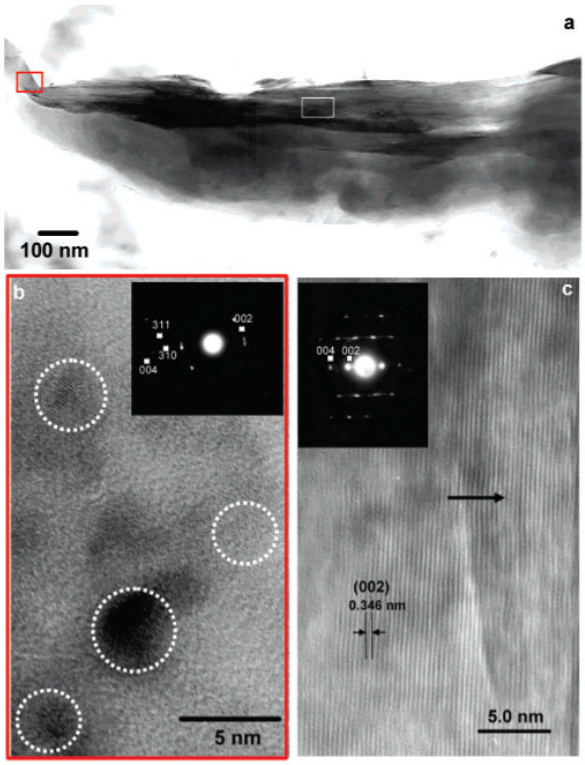

Figure 3.

High-resolution TEM characterization of the ribbon-like microstructures formed in the presence of 5.0 μg mL^{-1} amelogenin (σ_{OCP} = 1.45, pH 6.800, and 37 °C). (a) TEM image of one part of a ribbon. (b) HRTEM image taken from the tip of a ribbon (in the red rectangle marked in Figure 3a), revealing that the less mineralized area of the ribbons consists of nanocrystallites ~3-4 nm in diameter and indicated by dotted circles. The SAED pattern taken from this red rectangular region of a ribbon confirmed that the microstructure was HAP (inset). (c) HRTEM image taken from a white rectangular region of a ribbon in Figure 3a. The inset SAED pattern also confirmed that the ribbon-like structure was HAP. The measured lattice spacing ~0.346 nm corresponds to the (002) HAP lattice plane. Long arrow indicates the long axis direction of the ribbon-like microstructures.

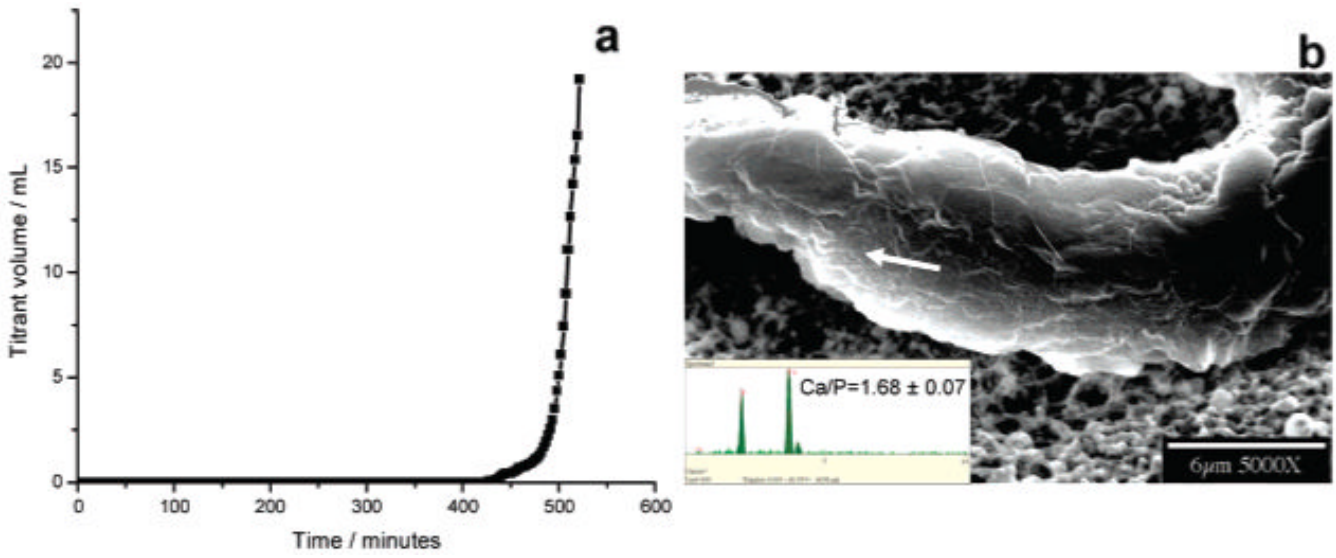

Figure 4.

CC Crystal growth of apatite. (a) Plot of titrant addition as a function of time for apatite crystal growth in the presence of 5.0 μg mL^{-1} amelogenin. (b) SEM of an ordered and thickened ribbon-like crystal. Arrow shows the direction of the orientation along the long axis of the ribbon-like microstructures. EDS of the ribbon-like crystals showing a HAP Ca/P ratio of 1.68 ± 0.07 (n = 5, number of crystals) (σ_{OCP} = 1.45, pH 6.800, and 37 °C).

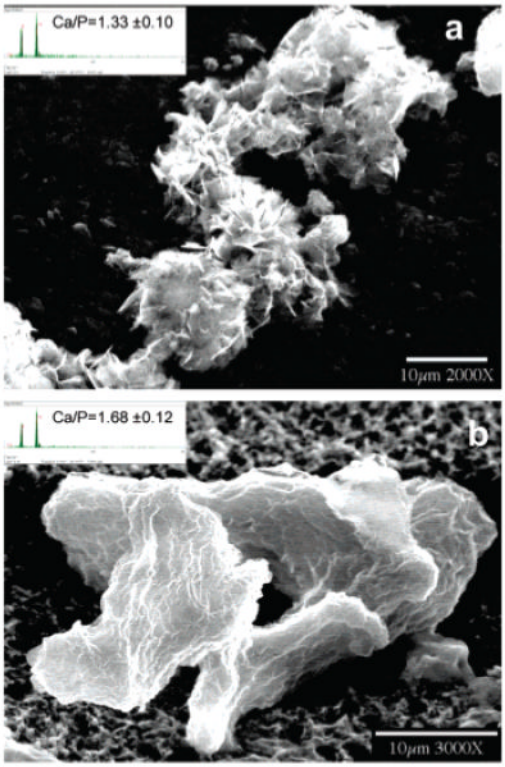

Figure 5.

Crystal morphological characterization at higher supersaturations. (a) SEM image of less ordered crystals formed in the absence of amelogenin. Inset figure is EDS of crystals, showing OCP Ca/P ratio of 1.33 ± 0.10 (n = 5, number of crystals). (b) SEM image of less ordered crystals formed in the presence of 5.0 μg mL^{-1} amelogenin. EDS (inset) of crystals showing a HAP Ca/P ratio of 1.68 ± 0.12 (n = 5, number of crystals) (σ_{OCP} = 2.32, pH 6.800, and 37 ° C).

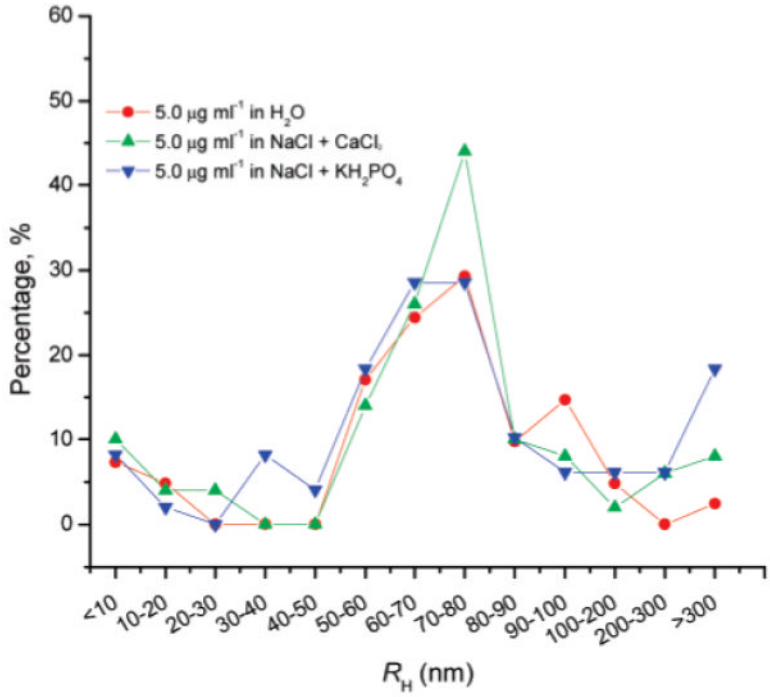

Figure 6.

Particle size distribution of rp172 assemblies by dynamic light scattering. The amelogenin protein (rp172) was dissolved in distilled water and diluted to 5.0 μg mL^{-1} in different solutions. The ionic concentrations were similar to those of the crystallization solutions. The pH of the calcium-containing solution was about 5.6 and that of the phosphate-containing solution was adjusted to 6.8 by the addition of potassium hydroxide. The large particles with R_H 60-80 nm were frequently detected. Small assemblies with R_H varying between 2.4 and 9.8 nm were occasionally detected.

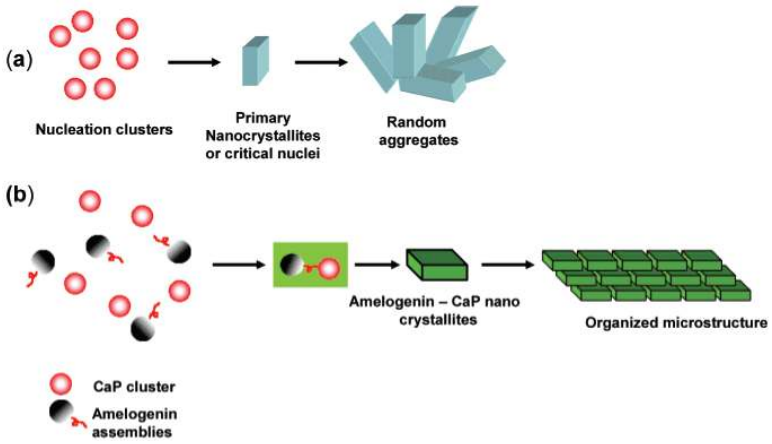

Figure 7.

A schematic illustration of apatite crystallization induced by amelogenin. (a) Random aggregates formed in the absence of amelogenin. (b) The organized microstructures are formed via co-assembly of amelogenin oligomers (small nanospheres) and apatite nanocrystallites. See text for details.